Fabrication of Ordered Ferromagnetic−Nonmagnetic Alloy Nanowire Arrays and their Magnetic Property Dependence on Annealing Temperature

Y. W. Wang,* L. D. Zhang, G. W. Meng, X. S. Peng, Y. X. Jin, and J. Zhang

Institute of Solid State Physics, Chinese Academy of Sciences, P.O. Box 1129, Hefei 230031, People's Republic of China

Received: August 10, 2001; In Final Form: December 8, 2001

Ordered ferromagnetic−nonmagnetic alloy (Co−Cu, Co−Ag and Fe−Ag) nanowire arrays embedded in the nanochannels of anodic aluminum membranes (AAM) have been fabricated by electrodeposition. Scanning electron microscopy and transmission electron microscopy observations reveal that these alloy nanowires are uniform in diameter and ordered. Magnetic measurements show that the perpendicular coercivity ($H_C^{\perp}$) of these ordered nanowire arrays increases dramatically, reaches their maximum, and then decreases sharply during the annealing process. However, there is not much change of the parallel coercivity ($H_C^{\parallel}$) for these alloy nanowire arrays in the same annealing conditions. This phenomenon should be contributed to the special structure of the nanowires/AAM.

1. Introduction

In recent years, one of the most interesting and intensely investigated classes of materials has been that of magnetic films and nanowires, due to not only the fundamental interest in these materials but also the potential applications of some of their properties.[1] In particular, the fabrication of ordered magnetic metal nanowire arrays has attracted considerable scientific and commercial attention due to their potential utilization in magnetic recording.[2,3] For example, nanoscale patterned arrays have been suggested as recording media to achieve recording densities of more than 100 Gbit/in.^{2}, each memory unit being stored in a single array.[4,5] This storage density is much higher than that of current commercial hard disks (3.7 Gbit/in^2) and also beyond the projected thermal limit of 40 Gbit/in.^{2} in continuous magnetic film.[6] We know that the coercivity and remanence of nanowire arrays of Fe,[7,8] Co,[9] Ni,[9,10] and ferromagnetic alloy such as Co−Ni, Fe−Ni, and Fe−Co electrodeposited in the alumite films[11] have been investigated in detail. In addition, various multilayered nanowires including Co/Cu,[12,13] NiFe/Cu,[13,14] CoNi/Cu[15] and Ni/Cu[16] have been studied intensively. Heterogeneous ferromagnetic−nonmagnetic alloy films such as Co−Cu and Co−Ag[17−19] grown by a variety of methods have also been investigated in detail. However, as far as we know, only a few studies on heterogeneous ferromagnetic−nonmagnetic alloy nanowire arrays systems exist in the literature. Among them, Bjythe et al. and Schwarzacher et al. have fabricated Co−Cu alloy nanowires into track-etched polymer membranes or alumite films by electrodeposition and presented a preliminary study of their transport property.[20,21] In our manuscript, we have successfully fabricated a series of ferromagnetic−nonmagnetic alloy nanowire arrays in AAM and studied their annealing temperature dependence of magnetic properties in detail. Moreover, magnetic measurements show that the perpendicular coercivity of these ordered nanowire arrays increases dramatically, reaches their maximum, and then decreases sharply during the annealing process. However, there is not much change of the parallel coercivity for these alloy nanowire arrays in the same annealing conditions. These results have not been reported in the publicized journal till now. In this work, we used the anodic aluminum membranes (AAM) as a template to fabricate the ferromagnetic−nonmagnetic alloy nanowire arrays via electrodeposition. Because the AAM has two significant advantages over the track-etched polymer membranes used in the fabrication of ordered nanostructures. First, it is well-known that the AAM grown in acid electrolytes possesses hexagonally ordered porous structures with nanochannel density in the range $10^{11}-10^{13}$/cm^2.[22] Second, the AAM is stable at higher temperature,[23] which opens up the possibility of studying how annealing modifies the magnetic properties of alloy nanowires. In this paper, ordered ferromagnetic−nonmagnetic alloy (Co−Cu, Co−Ag, and Fe−Ag) nanowire arrays embedded in the nanochannels of AAM have been successfully fabricated by electrodeposition, and the annealing temperature dependence of their magnetic properties has been studied.

2. Membranes Used

The AAM used as template in this work was prepared by using a two-step anodization process[24] to oxidize aluminum in acid solutions. The aluminum plates (99.999% purity, 0.3 mm thickness) were degreased in acetone and then annealed in a vacuum of about 10^{-5} Pa at 400 °C for 4 h to remove the mechanical stress and recrystallize. Then the aluminum plate was electropolished under a constant current condition of 90 mA/cm^2 for 3 min in a mixture of $HClO_4$ and C_2H_2OH at room temperature to smooth the surface morphology.

The aluminum plate was anodized in 0.3M oxalic acid ($C_2H_2O_4$) electrolyte. The anodizing voltage was 40 V and the temperature of the electrolyte was kept constant at 17 °C. After 3 h anodization, the plates were immersed in a mixture of 6 wt % H_3PO_4 and 1.8 wt % H_2CrO_4 at 60 °C for 7 h to remove the alumina layers. Then, the aluminum plate was anodized again for 6 h under the same conditions as the first step. At the bottom of the AAM were the remaining aluminum layers, which could be removed in a saturated $HgCl_2$ solution. A subsequent etching treatment was carried out in a 6 wt % H_3PO_4 at 30 °C for 70 min to remove the barrier layer on the bottom side of the AAM. The morphology of the as-prepared AAM was observed using an atomic force microscope [(AFM) Park Scientific Instruments, Autoprobe CP] and shown in Figure 1. From Figure 1, the almost perfect hexagonally arranged nanochannels with diameter about 60 nm and interchannel distance about 40 nm can be seen for AAM. The dark parts

* To whom correspondence should be addressed: E-mail: ywwangcn@china.com. Fax: +551-559-1434.

10.1021/jp013115d CCC: $22.00
Published on Web 02/16/2002

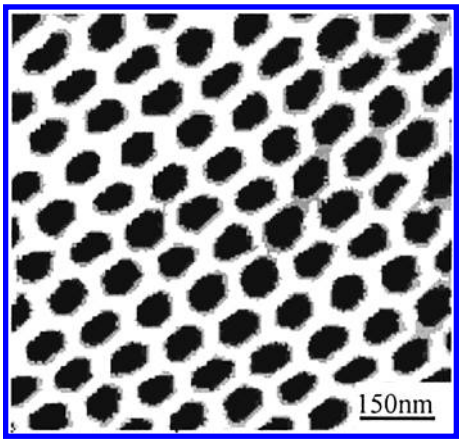

Figure 1. AFM photograph of surface of porous AAM prepared in 0.3 M $C_2H_2O_4$.

TABLE 1: Electrolytes and Electrodeposition Conditions of Co−Cu, Fe−Ag, and Co−Ag Alloy Nanowire Arrays

electrolytes (g/L)	Co−Cu	Fe−Ag	Co−Ag
$CoSO_4 \cdot 7H_2O$	50		40
$CuSO_4 \cdot 5H_2O$	0.5		
$AgNO_3 \cdot 7H_2O$		20	50
$FeSO_4 \cdot 5H_2O$		20	
CH_3COONH_4		10	40
$Na_2S_2O_3 \cdot 5H_2O$		100	
Na_2SO_3		40	
H_3BO_3	40		
NH_3H_2O			60

electrodeposition conditions	Co−Cu	Fe−Ag	Co−Ag
current density (mA/cm^2)	1.5	2.5	1.5
time (h)	6	6	6
temp (^{o}C)	room temp	room temp	room temp

correspond to the nanochannels. Optical microscope measurements show that the thickness of our AAM is about 50 μm. The aspect ratios (depth to diameter) of the nanochannels of AAM are about 1000.

3. Experimental Procedures

3.1. Fabrication and Annealing. A layer of Au was sputtered onto one side of the AAM serving as the working electrode in a two-electrode electrochemical cell. The electrolytes and the electrodeposition conditions of Co−Cu, Fe−Ag, and Co−Ag alloy nanowire arrays were listed in Table 1. The electrodeposition was carried out at a constant current density, with carbonate serving as the counter electrode. After electrodeposition, these ordered alloy nanowire arrays embedded in AAM were annealed at different temperatures T_A (300, 400, 500, and 600 °C) for 1 h in furnace under a flowing Ar atmosphere, respectively. The magnetic properties were measured by a vibrating sample magnetometer (Lakeshore, VSM-5s-15), with the applied field either parallel or perpendicular to the surface of the samples. The coercivity (H_C) and the saturation magnetization (M_S) were obtained from these hysteresis loops.

3.2. Sample Preparation for SEM and TEM Observations. For observation under a scanning electron microscope [(SEM) JEOL JSM-6300], small pieces of AAM with these ordered alloy nanowire array samples were eroded by an aqueous solution of 5 wt % NaOH for 5−10 min in order to remove the upper part or whole AAM. Then they were washed with distilled water several times and dried in air.

The morphology of these alloy nanowires was obtained by transmission electron microscope [(TEM) JEM-200CX] after completely dissolving AAM in an aqueous solution of 5 wt % NaOH. Some of these alloy nanowires remained in the solution.

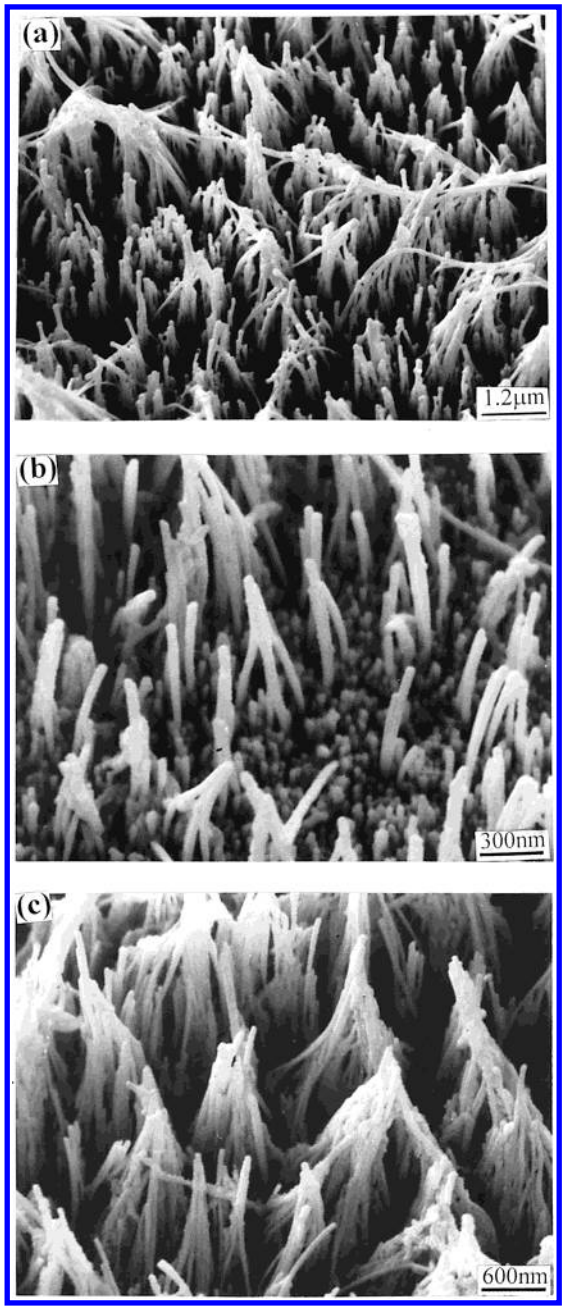

Figure 2. Typical top-view SEM images showing the general morphology of the ferromagnetic−nonmagnetic alloy nanowire arrays: (a) Co−Cu; (b) Fe−Ag; (c) Co−Ag.

A drop of the solution was placed on a Cu grid with a carbon film and allowed to dry prior to electron microscope analysis, respectively.

The chemical compositions of these alloy nanowire arrays were determined by energy dispersed X-ray spectrometer (EDS), and their phase structural characterizations were carried out by X-ray diffraction [(XRD) MXP18AHF].

4. Results and Discussion

4.1. Morphology and Phase Structural Characterizations. The typical top view (shown in Figure 2a−c, respectively) and cross-section (shown in Figure 3a−c, respectively) SEM images of Co−Cu, Fe−Ag, and Co−Ag nanowire arrays demonstrate that these deposited alloys, indeed, fill the nanochannels of the AAM uniformly and that the nanowires are apparently continuous, parallel, and ordered. The measured diameters of these alloy

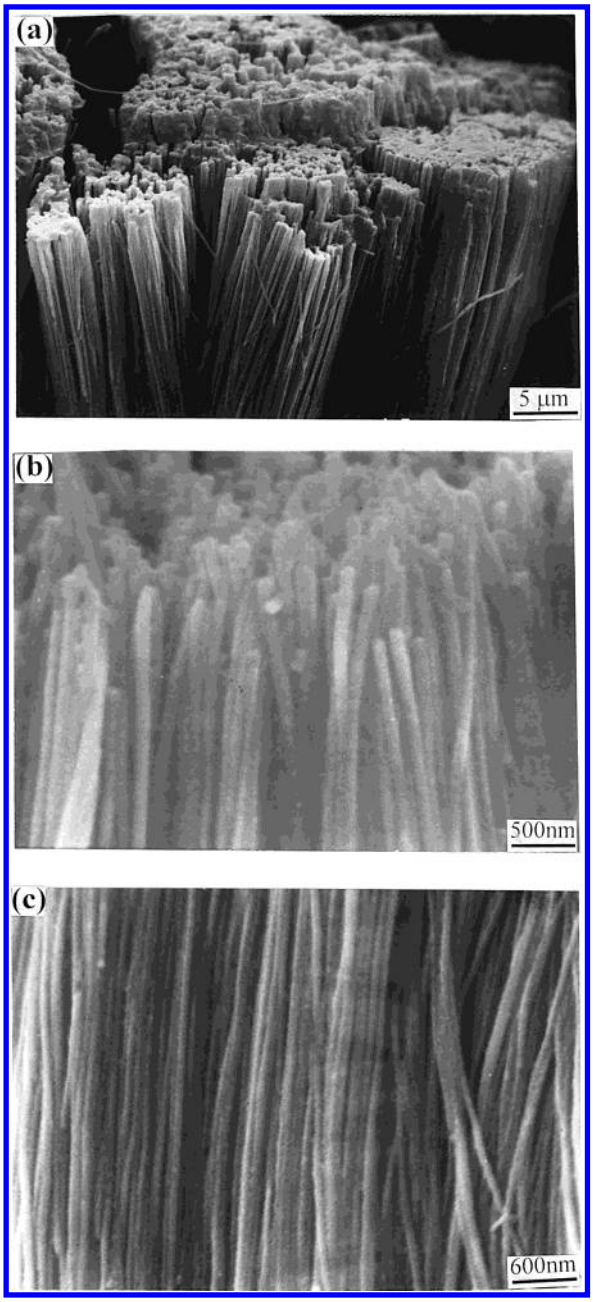

Figure 3. Typical cross-section SEM images showing the general morphology of the ferromagnetic−nonmagnetic alloy nanowire arrays: (a) Co−Cu; (b) Fe−Ag; (c) Co−Ag.

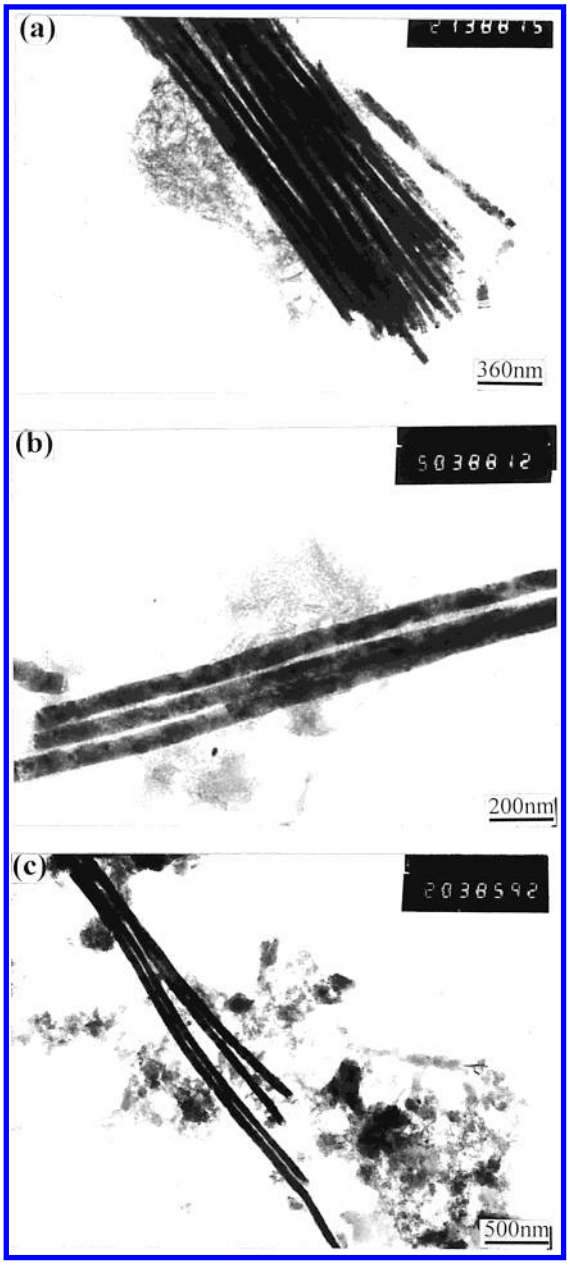

Figure 4. TEM images of the alloy nanowires liberated from AAM: (a) Co−Cu; (b) Fe−Ag; (c) Co−Ag.

nanowires corresponded closely to the nanochannel diameters. From Figure 2, it can be estimated that the density of these alloy nanowires is about $10^{11}-10^{13}/cm^2$, which shows the great opportunities to the magnetic recording. The TEM images of Co−Cu, Fe−Ag, and Co−Ag nanowires liberated from the AAM are shown in Figure 4a−c, respectively. It can be seen that these alloy nanowires are uninterrupted with diameter about 60 nm, which correspond to the nanochannel diameter of the AAM used. Energy dispersed X-ray spectrometer (EDS) analysis attached on SEM demonstrates that the atomic ratio of Co and Cu, Fe and Ag, and Co and Ag in the corresponding nanowires are close to 20:80, 20:80, and 14:86 (shown in Figure 5a−c, respectively). The Co−Cu, Fe−Ag, and Co−Ag diffraction spectra of the as-deposited nanowire arrays embedded in AAM (shown in Figure 6a−c, the bottom curves) also indicate that these lines correspond to the face centered cubic (fcc) Cu, fcc-Ag, and fcc-Ag structure, respectively.

We know that, under equilibrium conditions, the mutual solubility of ferromagnetic and nonmagnetic metal is very low in both the solid and liquid forms, such as Co and Cu, Co and Ag, and Fe and Ag. However, under nonequilibrium conditions, the Co/Cu, Fe/Ag, and Co/Ag systems could form metastable solid solutions. In this type of material, the annealing treatment results in the recrystallization of these metastable alloys into two separate phases, leading to the formation of small ferromagnetic metal particles that exhibit greatly enhanced magnetic properties because of their single-domain nature.[25] These processes have already been proved by XRD and are shown in Figure 6. It can be seen that the as-deposited samples are single-phase fcc-Cu, fcc-Ag, and fcc-Ag, respectively, but the Cu and Ag diffraction lines are shifted toward higher angles. Therefore the as-deposited alloy nanowire arrays in this work are solid solutions. As shown in Figure 6a, the fcc-Cu structure is preserved up to $T_A = 400$ °C. With further annealing at 500 °C, however, the fcc-Co lines appear, indicating the recrystallization of the metastable Co-Cu alloy into fcc-Co and fcc-Cu.

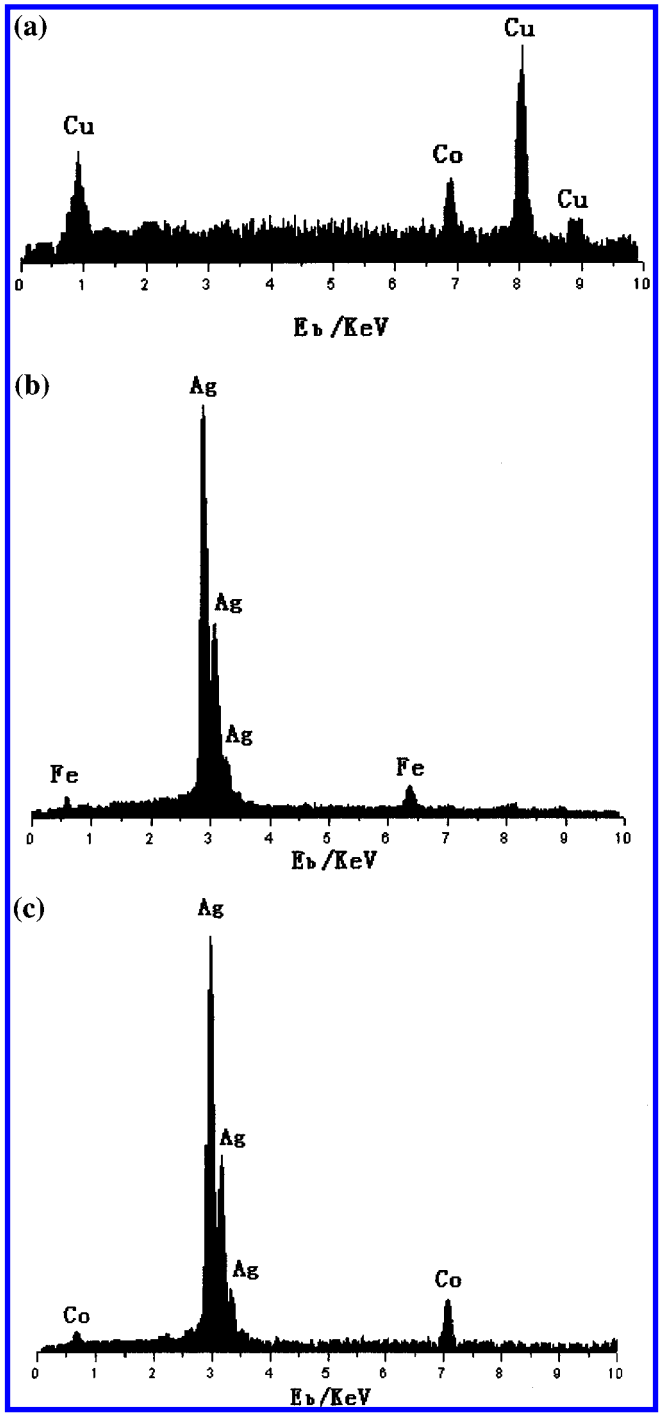

Figure 5. Energy-dispersed X-ray analysis spectra of the alloy nanowires in Figure 1: (a) Co−Cu; (b) Fe−Ag; (c) Co−Ag.

As T_A increased over 500 °C, the diffraction lines became progressively narrower due to the growth of particle size. Figure 6b indicates that the fcc-Ag structure is not changed up to T_A = 300 °C. With further annealing at 400 °C, however, the body centered cubic (bcc) α-Fe lines appear, indicating the recrystallization of the metastable Fe-Ag alloy into fcc-Ag and bcc-Fe. As T_A increased over 400 °C, the diffraction lines became progressively narrower. The phase structural characterizations of the Co−Ag alloy nanowire arrays during the annealing process have been shown in Figure 6c. The fcc structure is preserved up to T_A = 300 °C. With further annealing at 400 °C, however, the fcc-Co lines appear, indicating the recrystallization of the metastable Co−Ag alloy into fcc Co and fcc

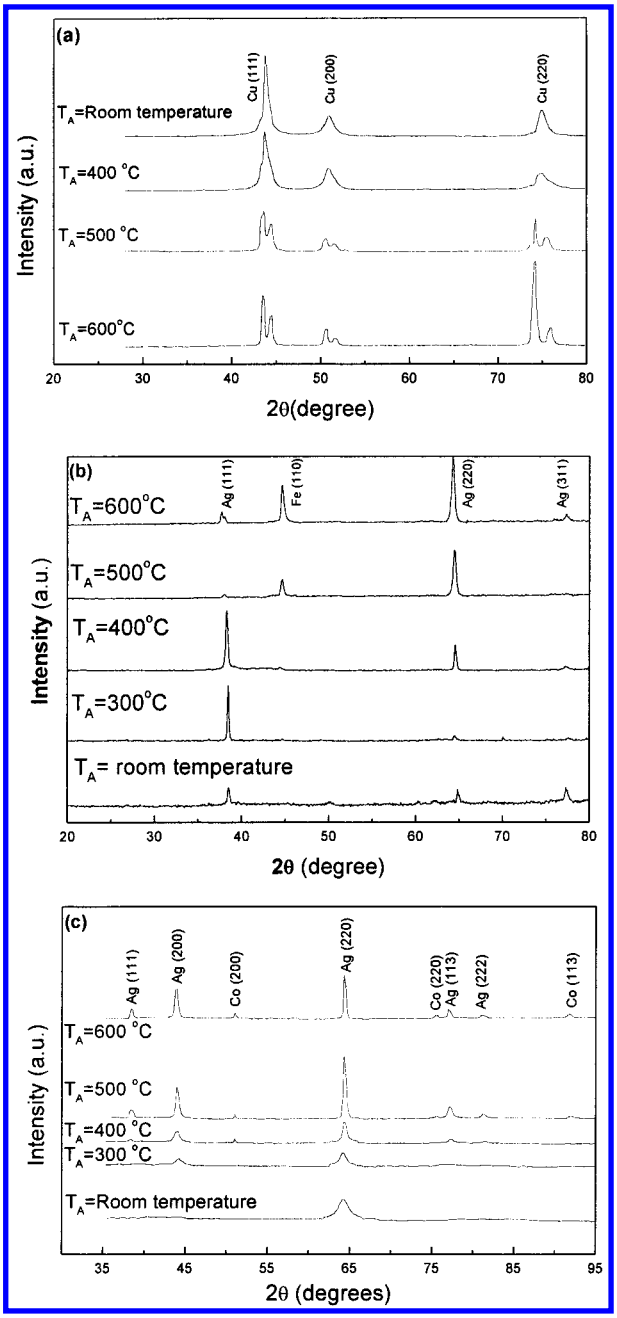

Figure 6. X-ray diffraction spectra of the alloy nanowire arrays at room temperature, after annealing for 1 h at various temperatures T_A: (a) Co−Cu; (b) Fe−Ag; (c) Co−Ag.

Ag. As T_A increased over 400 °C, the diffraction lines became progressively narrower due to the growth of particle size.

4.2. Magnetic Properties. *4.2.1. Coercivity.* The effect of T_A on the coercivity measured at room temperature is shown in Figure 7a−c for $Co_{20}Cu_{80}$, $Fe_{20}Ag_{80}$, and $Co_{14}Ag_{86}$ alloy nanowire arrays embedded in AAM, respectively. At first, we note that the coercivity measured with the external field applied perpendicular to the sample surface ($H_C^{\perp}$) is always larger than that of the parallel one ($H_C^{\parallel}$) in all figures, due to the preferential orientation of the nanowires.[26]

As shown in Figure 7a, the perpendicular coercivity ($H_C^{\perp}$) of the ordered $Co_{20}Cu_{80}$ nanowire arrays embedded in AAM increases dramatically with T_A over 300 °C, reaches its maximum (429.1 Oe) at 500 °C, and then decreases sharply as T_A is increased further. Parts b and c of Figure 7 reveal that the temperature dependence of $H_C^{\perp}$ for the ordered $Fe_{20}Ag_{80}$ and $Co_{14}Ag_{86}$ alloy nanowire arrays. It can be seen that the $H_C^{\perp}$

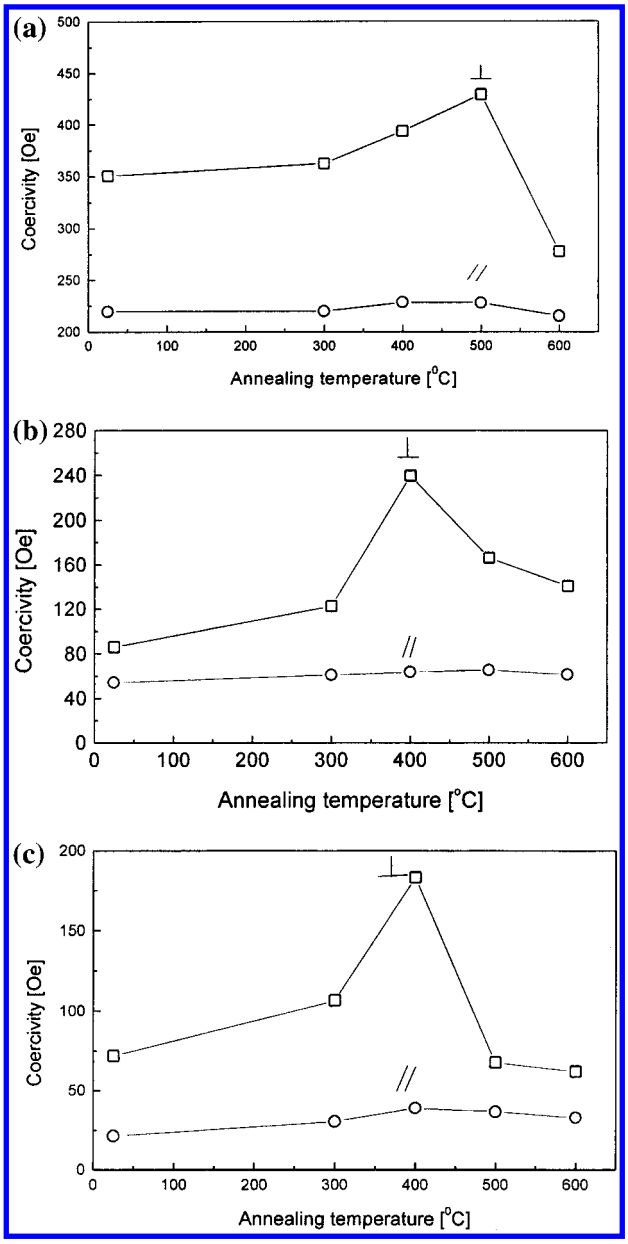

Figure 7. Room-temperature coercivity of the nanowire arrays embedded in AAM as a function of annealing temperature T_A, measured with the external field applied parallel (∥, circles) and perpendicular (⊥, squares) to the surface of the samples: (a) Co−Cu; (b) Fe−Ag; (c) Co−Ag.

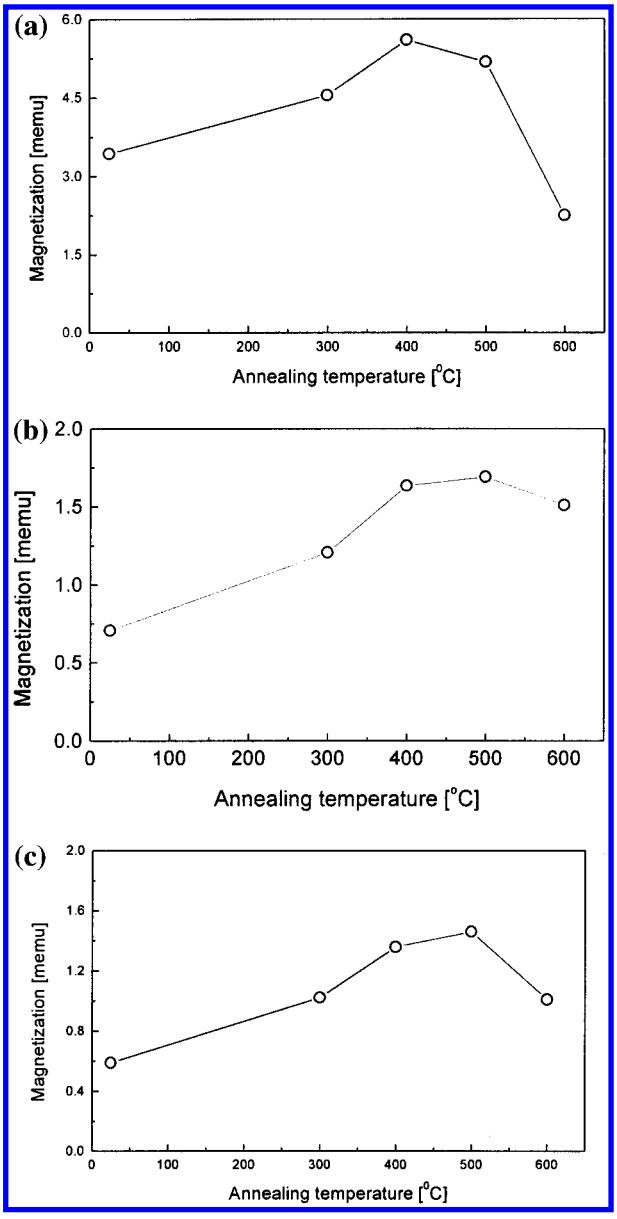

Figure 8. Room-temperature saturation magnetization as a function of annealing temperature T_A: (a) Co−Cu; (b) Fe−Ag; (c) Co−Ag.

variety tendency of these alloy nanowire arrays with an increase of annealing temperature is the same as that of $Co_{20}Cu_{80}$ alloy nanowire arrays. These phenomena are similar to these of the Co−Cu, Fe−Ag, and Co−Ag alloy films .[17−19] As T_A is increased, a very small change occurs in $H_C^{\perp}$, until the temperature where an obvious increase in $H_C^{\perp}$ is seen. So this phenomenon can be attributed to the appearance of a small, single domain ferromagnetic metal such as Co, Fe precipitates formed in these ferromagnetic−nonmagnetic alloy nanowire arrays. As T_A is further increased, these ferromagnetic metal grains grow larger in size, leading to the increase of $H_C^{\perp}$. This tendency continues until the critical size for these single domain particles is exceeded or when most of the particles begin to coalesce. The maximum perpendicular coercivities of $Co_{20}Cu_{80}$, $Fe_{20}Ag_{80}$, and $Co_{14}Ag_{86}$ nanowire arrays embedded in AAM are about 239.5, 429.1, and 183.1 Oe at 500, 400, and 400 °C, respectively. But $H_C^{\perp}$ decreases as T_A is further increased over the temperature where the $H_C^{\perp}$ is maximal. This is most likely to happen when ferromagnetic metal grains come in contact and begin to sinter together.

In addition, we can see that, with the increase of annealing temperature, the change has not been observed in $H_C^{\parallel}$ in Figure 7, which is much different from that in the ferromagnetic−nonmagnetic alloy films. This may be attributed to the structural difference between the films and the nanowires. We know that the ferromagnetic metal particles will form and grow along every direction of the ferromagnetic−nonmagnetic alloy films in the annealing processes, which makes contribution to not only $H_C^{\perp}$ but also $H_C^{\parallel}$. But the ordered ferromagnetic−nonmagnetic alloy nanowires with high aspect ratios (length to diameter, about 1000) in AAM are separated from each other, namely the nanowires have highly anisotropic structure. Hence the formation and growth of the ferromagnetic metal particles will be limited along the direction parallel to the nanowires in the annealing process, which makes a great contribution to $H_C^{\perp}$, but little to $H_C^{\parallel}$.

4.2.2. Saturation Magnetization. Figure 8a−c show the saturation magnetization (M_S) measured at room temperature

as a function of annealing temperature for $Co_{20}Cu_{80}$, $Fe_{20}Ag_{80}$, and $Co_{14}Ag_{86}$ alloy nanowire arrays embedded in AAM, respectively. Figure 8a indicates that, as T_A rises, an increase in the saturation magnetization of $Co_{20}Cu_{80}$ nanowire arrays is seen and the maximum saturation magnetization is $M_S = 5.6$ memu at $T_A = 400$ °C. However, the value of M_S decreases as T_A is further increased. Figure 8b also shows that, as T_A rises, an increase in the saturation magnetization of $Fe_{20}Ag_{80}$ nanowire arrays is seen, the maximum saturation magnetization is $M_S = 1.69$ memu at $T_A = 500$ °C, and M_S decreases as T_A is further increased. The M_S variety tendency of $Co_{14}Ag_{86}$ alloy nanowire arrays with an increase of annealing temperature is similar to those of $Co_{20}Cu_{80}$ and $Fe_{20}Ag_{80}$ nanowire arrays. And the maximum saturation magnetization is $M_S = 1.46$ memu at $T_A = 500$ °C. The tendency of M_S for $Co_{20}Cu_{80}$, $Fe_{20}Ag_{80}$, and $Co_{14}Ag_{86}$ alloy nanowire arrays caused by the changes of these ferromagnetic metal particles in the annealing process is the same as the perpendicular coercivity. We noted that the increase of M_S begins at temperatures lower than the one at which the coercivity starts to rise. In this regard, we think that the increase of M_S just begins as the ferromagnetic metal atoms begin to cluster during the annealing process. Thus the initial clustering enhances the M_S, but the coercivity is not affected until the ferromagnetic metal precipitates grow larger in size.

5. Conclusion

In conclusion, ordered Co−Cu, Fe−Ag, and Co−Ag alloy nanowire arrays were successfully fabricated in the nanochannels of AAM by electrodeposition. The SEM and TEM observations indicate that these ordered ferromagnetic−nonmagnetic alloy nanowire arrays are apparently continuous, parallel, and ordered. Magnetic measurements show that the perpendicular coercivity ($H_C^{\perp}$) of these ordered nanowire arrays embedded in AAM increases dramatically as annealing temperature (T_A) rises, reaches their maximum at one temperature, and then decreases sharply as T_A rises further. However, there is not much change of the parallel coercivity ($H_C^{\parallel}$) for these alloy nanowire arrays in the same annealing conditions. This phenomenon should be attributed to the special structure of the nanowire arrays/AAM.

Acknowledgment. This work was supported by the Ministry of Sciences and Technology of China (Grant No. G1999064501) and the Natural Science Foundation of China (Grant No. 19974055).

References and Notes

(1) Blythe, H. J.; Fedosyuk, V. M. *Phys. Status Solidi (A)* **1994**, *142*, 13.

(2) Tonucci, R. J.; Justus, B. L.; Campillo, A. J.; Ford, C. E. *Science* **1992**, *258*, 783.

(3) Whitney, T. W.; Jiang, J. S.; Searson, P. C.; Chien, C. L. *Science* **1993**, *261*, 1316.

(4) White, R. M.; New, R. M. H.; Pease, R. F. W. *IEEE Trans. Magn.* **1996**, *33*, 990.

(5) Routkevitch, D.; Tager, A. A.; Haruyama, J.; Almawlawi, D.; Moskovits, M.; Xu, J. M. *IEEE Trans. Electron Dev.* **1996**, *43*, 1646.

(6) Lu, P. L.; Charap, S. H. *IEEE Trans. Magn.* **1994**, *30*, 4230.

(7) Lodder, J. C.; Chang-Zhang, L. *IEEE Trans Magn.* **1989**, *25*, 4171.

(8) Almawlani, D.; Coombs, N.; Moskovits, M. *J. Appl. Phys.* **1991**, *70*, 4421.

(9) Whitney, T. M.; Jiang, J. S.; Searson, P. C.; Chien, C. L. *Science* **1993**, *261*, 1316.

(10) Arai, K. I.; Ishiyama, K.; Ohoka, Y.; Kang, H. W. *J. Magn. Soc. Jpn.* **1989**, *13*, 789.

(11) Kawai, S.; Ishiguro, I. *J. Electrochem. Soc.* **1976**, *123*, 1047.

(12) Piraux, L.; George, J. M.; Despres, J. F.; Leroy, C.; Ferain, E.; Legras, R.; Ounadjela, K.; Fert, A. *Appl. Phys. Lett.* **1994**, *65*, 2484.

(13) Blondel, A.; Meir, J. P.; Doudin, B.; Ansermet, J. P. *Appl. Phys. Lett.* **1994**, *65* 1994 3020.

(14) Duboris, S.; Marchal, C.; Beuken, J. M.; Piraux, L.; Duvail, J. L.; Fert, A.; George, J. M.; Maurice, J. M. *Appl. Phys. Lett.* **1997**, *70*, 396.

(15) Atterborough, K.; Hast, R.; Schwarzacher, W.; Ansermet, J. P.; Blondel, A.; Doudin, B.; Meier, J. P. *Mater. Res. Soc. Symp. Proc.* **1995**, *384*, 3.

(16) Wang, L.; Yu-Zahng, K.; Metrot, A.; Bonhomme, P.; Troyon, M. *Thin Solid Films* **1996**, *288*, 86.

(17) Childress, J. R.; Chien, C. L. *Appl. Phys. Lett.* **1990**, *56*, 95.

(18) Fert, A.; Piraux, L. *J. Magn. Magn. Mater.* **1999**, *200*, 338.

(19) Liou, S. H.; M alhotra, S.; Shan, Z. S.; Sellmyer, D. J.; Nafis, S. *J. Appl. Phys.* **1991**, *70*, 5882.

(20) Blythe, H. J.; Fedosyuk, V. M.; Kasyutich, O. I.; Schwarzacher, W. *J. Magn. Magn. Mater.* **2000**, *208*, 251.

(21) Schwarzacher, W.; Kasyutich, O. I.; Evans, P. R.; Darbyshire, M. G.; Yi, G.; Fedosyuk, V. M.; Rousseaut, F.; Gambril, E.; Deanini, D. *J. Magn. Magn. Mater.* **1999**, *185*, 198.

(22) Masuda, H.; Fukuda, K. *Science* **1995**, *268*, 1466.

(23) Evans, P. R.; Yi, G.; Schwarzacher, W. *Appl. Phys. Lett.* **2000**, *76*, 481.

(24) Mausda, H.; Satoh, M. *Jpn. J. Appl. Phys.* **1996**, *35*, 1126.

(25) Morrish, A. H. *The Physical Principles of Magnetism*; Wiley: New York, 1965.

(26) Childress, J. R.; Chien, C. L. *J. Appl. Phys.* **1991**, *70*, 5885.